MATHEMATICAL MODELING OF THE FORCE REQUIRED TO MOVE PLATFORMS INTENDED FOR SOIL SAMPLING
/
MODELAREA MATEMATICĂ A FORȚEI NECESARE DEPLASĂRII PLATFORMELOR DESTINATE PRELEVĂRII PROBELOR DE SOL

Mario CRISTEA [1], Mihai Gabriel MATACHE [1], Robert-Dorin CRISTEA *[1], Andreea-Iulia GRIGORE [1], Laurențiu VLĂDUȚOIU [1]

[1] National Institute of Research - Development for Machines and Installations Designed to Agriculture and Food Industry – INMA Bucharest / Romania;

*) *E-mail: robertcri@yahoo.com*

DOI: https://doi.org/10.35633/inmateh-74-44

Keywords: *self-propelled platform, soil sampling, traction force, mathematical model.*

ABSTRACT

Self-propelled platforms designed for soil sampling represent a remarkable technological advancement in the field of soil research, providing efficient and precise collection of essential data regarding soil composition. These platforms are equipped with advanced technologies and sophisticated sampling systems, offering researchers the opportunity to obtain detailed data in an automated and replicable manner. In this article, the technical features of self-propelled platforms for soil sampling and their significance in advancing soil sciences research will be investigated.

In this paper, a mathematical model is described to aid in the design of the propulsion system of self-propelled platforms intended for soil sample collection under conditions of movement on horizontal or sloping terrain. With this mathematical model, the forces required for the platform to move can be calculated, considering the constraints specific to each project. When the project is completed, and key parameters such as the total weight of the platform, dimensions, payload weight, and transmission gear ratios are known, the minimum power required for the engine to move the platform can be calculated.

REZUMAT

Platformele autopropulsate destinate prelevării probelor de sol reprezintă un avans tehnologic remarcabil în domeniul cercetării solului, furnizând o colectare eficientă și precisă a datelor esențiale privind compoziția solului. Aceste platforme sunt dotate cu tehnologii avansate și sisteme de eșantionare sofisticate, oferind cercetătorilor oportunitatea de a obține date detaliate într-un mod automatizat și reaplicabil. În acest articol, vom explora în profunzime caracteristicile tehnice ale platformelor autopropulsate destinate prelevării probelor de sol, precum și importanța lor în avansarea cercetărilor în domeniul științelor solului. În această lucrare este descris un model matematic care ajuta la proiectarea sistemului de propulsie a platformelor autopropulsate destinate prelevării probelor de sol în condițiile de deplasare pe un teren orizontal sau un teren aflat în pantă. Cu ajutorul acestui model matematic se pot calcula forțele de care este nevoie ca platforma să execute o deplasare ținând cont de constrângerile care se impun la fiecare proiect în parte. Atunci când este realizat proiectul și sunt cunoscute, de exemplu, greutatea totală a platformei, dimensiunile dar și greutatea utilă și rapoartele de transmitere ale transmisiei, se poate calcula puterea minimă necesară pentru motor ca platforma să se poată deplasa.

INTRODUCTION

Self-propelled platforms designed for soil sampling are an innovative paradigm in soil research, providing an advanced and precise method for collecting essential data on soil composition and properties. These technologically advanced vehicles have become the focal point for researchers in the soil sciences, enabling detailed and accurate data collection, with a significant impact on understanding pedological processes and the practical application of research results (*Oprescu R.M. et al, 2023*).

Self-propelled platforms benefit from rapid advancements in autonomous system technologies, robots, sensors, and navigation algorithms. For the navigation of self-propelled platforms in open or enclosed spaces, the development of computational models is necessary to enable movement under conditions of maximum safety and the utilization of optimized routes (*Ibrahim A. et al., 2023*). These not only facilitate data collection but also make significant contributions to optimizing research processes in the field of soil studies (*Zawilski, B.M. et al, 2023*).

Using mathematical models of precise movement of self-propelled platforms on agricultural land, simulation models can be created to increase efficiency, but also to reduce soil damage (*Bulgakov V. et al, 2018*). It can also simulate the pressure exerted by self-propelled platforms equipped with various agricultural machinery, such as sprayers (*Li W. et al, 2022*).

The evolution of self-propelled platforms has been substantial in recent years, transitioning from simple devices to sophisticated and intelligent vehicles. The use of autonomous robots in soil research has marked a significant leap in data collection, facilitating access to challenging areas and ensuring increased accuracy in sample collection. This technological evolution has been fueled by advanced research in the fields of artificial intelligence and navigation algorithms (*Vaeljaots F. et al, 2018*).

An essential aspect of self-propelled platforms is represented by their advanced sampling systems. These systems are designed to collect representative samples, taking into account the specific characteristics of the soil, such as texture, water content, and chemical composition. Specialized sensors and integrated tools enable researchers to obtain detailed information about the physical and chemical properties of the soil in real-time (*Huuskonen J., Oksanen T., 2018; Tan K.H., 2005*).

The use of self-propelled platforms in soil research has a significant impact on agricultural resource management. The collected data provides essential information for optimizing agricultural practices, including irrigation needs, fertilizer application, and chemical substance management. This personalized approach contributes to resource efficiency and reduces environmental impact (*Vlăduţ V. et al, 2020*).

While the agricultural sector has made significant progress in implementing robotic automation in various processes, there are still notable challenges associated with mechanization in specific environments and techniques, such as vineyard cultivation and orchard management in mountainous or steep terrain. These challenges stem from difficult topographic conditions, extreme fragmentation of vineyards, variability in weather conditions, rich biodiversity, and other concomitant factors. Real-time tracking of soil robots in environments like forests, pastures, and vineyards has seen the development of environmental detection methods using YOLO (You Only Look Once) and a multi-target tracking algorithm designed for monitoring ground robot activities through real-time digital video transmissions (*Cao X. et al., 2023*). In the context of this complexity, farmers show an increased interest in implementing precision spraying/mowing robots characterized by financial efficiency, operational safety, and autonomy, with the ability to operate effectively in vineyards situated on steep slopes. The purpose of these efforts is to reduce costs, optimize agricultural process efficiency, and minimize the negative impact on the environment associated with agricultural activities (*Vanghele N.A. et al, 2021*).

Air Technical Industries (ATI), based in Mentor, Ohio, has designed and developed a self-propelled platform with remarkable capabilities (figure 1) (*https://www.mhnetwork.com/self-propelled-platform-truck-tug/*).

Fig. 1 - Air Technical Industries platform

The propulsion of this platform is provided by an electric motor powered by a 24-volt nominal voltage battery.

The fruit harvesting device ARGILÉS AF-5 (figure 2) is equipped with a Kubota 3-cylinder, 25-horsepower engine. Its operation can be managed through a radio remote control, providing the user with flexible control over the machine.

Fig. 2 - ARGILÉS AF-5, Machine for fruit picking, cutting, thinning, hail netting, etc.
(https://argiles.es/informacion-producto/af5/?lang=en)

Additionally, this machine exhibits a maximum speed of 14 km/h, contributing to the efficiency and speed of the fruit harvesting process (https://argiles.es/informacion-producto/af5/?lang=en).

Fig. 3 - UGV Robotics Plus
(https://www.powermotiontech.com/sensors-software/automation/media-gallery/21254335/robotics-plus-unveils-unmanned-ground-vehicle-for-agricultural-operations?id=21254335&slide=2)

Through this Unmanned Ground Vehicle (UGV), also known as an autonomous ground vehicle, Robotics Plus aims to contribute to addressing the labor shortage issue faced by the contemporary agricultural industry. The vehicle in question has been designed in a compact format, facilitating maneuverability within tightly spaced row crops, characteristic of orchards, vineyards, and other similar agricultural applications. The use of an electric steering system and independent motors gives the UGV the ability to make turns on its rear axle (figure 3).

The implementation of a hybrid propulsion system, with diesel-electric power, is an advantage in reducing fuel consumption and emissions while maintaining sufficient power for the efficient execution of agricultural activities throughout the working day (https://www.powermotiontech.com/sensors-software/automation/media-gallery/21254335/robotics-plus-unveils-unmanned-ground-vehicle-for-agricultural-operations?id=21254335&slide=2).

Fig. 4 - OMNiDRIVE self-propelled platform
(https://www.agriculture.com/news/technology/raven-announces-new-product-brand-and-autonomous-growth-platform)

The self-propelled electric platform developed by OMNi, Raven – OMNiDRIVE (figure 4), shows the capability to efficiently replace certain agricultural machinery, thereby enabling farmers to perform various tasks throughout the growing season. Mission launches can be carried out both autonomously and through direct control from a tablet. A notable feature of this platform is the absence of dedicated personnel for its operation (*https://www.agriculture.com/news/technology/raven-announces-new-product-brand-and-autonomous-growth-platform*).

Fig. 5 - The smart mower R 150
(https://hse-uav.com/products/r150-2023-autonomous-tractor-mower)

Drawing on expertise in autonomous driving and artificial intelligence (AI) training, XAG has implemented new enhancements to its UGV R150 system (figure 5). The XAG R150 can be characterized as an "open and scalable utility-loading platform," capable of integrating various modules for activities such as precision spraying, fertilizing, and mowing of crops. The RevoMower 2.0 system, designed to facilitate grass cutting in complex terrestrial environments like farmlands, marshes, and orchards, is part of this platform. Equipped with a 6 kW power motor, the XAG R150 demonstrates the ability to efficiently control weeds and small shrubs *(https://hse-uav.com/products/r150-2023-autonomous-tractor-mower*).

Fig. 6 - UGV Husky
(https://clearpathrobotics.com/blog/2021/01/husky-ugv-drives-smart-precision-agriculture-for-steep-slope-vineyards/)

The AgRobIT project, based on the UGV Husky platform (figure 6), proposes a simplified architecture built on a ROS (Robot Operating System) stack solution, consisting of three main ROS packages: localization and mapping, path planning and control, and mission supervisor. AgRobIT has successfully used the achievements of INESCTEC over the past four years, including VineSLAM (a cost-effective, modular, and reliable localization system capable of working with or without available GNSS and integrating semantic information) and AgRobPP (path planning and control systems aware of soil compaction and the robot's center of gravity) (*https://clearpathrobotics.com/blog/2021/01/husky-ugv-drives-smart-precision-agriculture-for-steep-slope-vineyards*).]

MATERIALS AND METHODS

The mathematical model was developed using relationships describing vehicle dynamics since the platforms are subject to the same forces, moments, and efforts. The resulting mathematical model aims to determine the force required by a motor for the platform to move. A series of steps were followed to study the forces involved in all the mechanisms that make up the propulsion system. In general, the propulsion system consists of an engine, gearbox, final drive, and wheel or track. Most of the forces influencing movement occur at the wheel or track level. For this reason, the study method began with wheel kinematics.

Wheel kinematics is a branch of mechanics that deals with the study of the motion and behavior of wheel systems, including the analysis of relationships between wheel motion and associated parameters such as speed, acceleration, and position in space. This discipline is crucial in engineering, especially in fields involving the design of vehicles or other systems that utilize wheels, such as mobile robots, autonomous vehicles, or any other application involving the motion and orientation of wheels.

In the context of constant speed motion, figure 7, the wheels experience the torque M_R and the gravitational force or the load on the wheel G_R (acting perpendicular to the direction of motion and applied at the center of the wheel). As a result of the interaction of these two loads, the rolling resistance reaction Z_R, the traction force F_t, and the friction force X occur (*Băisan, 2020*).

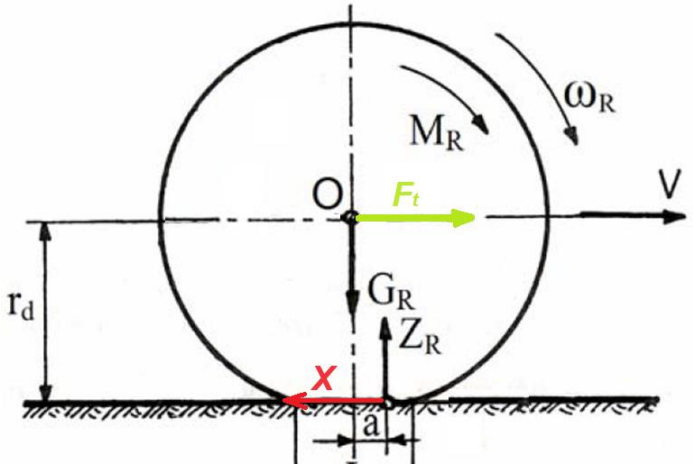

Fig. 7 - Equilibrium of the drive wheel on a non-deformable roadway (Băisan, 2020)

As, upon contact with the rolling surface, the wheel undergoes deformation along the length L, and the pressure forces are not symmetrical, the Z_R reaction will experience a displacement at a distance from the wheel's vertical axis.

The equilibrium equations *(Băisan, 2020)* in the case of constant speed rolling can be expressed by:

$$X - F_t = 0 \quad (1)$$

$$Z_R - G_R = 0 \quad (2)$$

$$X\, r_d + Z_R\, a - M_R = 0 \quad (3)$$

From equations (1), (2), and (3) follows the relationship:

$$X = \frac{M_R}{r_d} - Z_R \frac{a}{r_d} \text{ [N]} \quad (4)$$

where:

X – friction force [N]; F_t – tractive force [N]; Z_R – reaction force [N]; G_R – load on the wheel [N]; M_R – wheel torque [Nm]; r_d – dynamic wheel radius [m]; a – distance by which the reaction force Z_R is shifted forward [m].

In the scenario of a wheel rolling on a deformable track, figure 8, while maintaining a constant speed, it is assumed that the deformation involves the existence of a cylindrical surface in front of the wheel and a flat surface behind it. Distinct forces and reactions act on the wheel in this configuration, namely R_1 on the cylindrical surface and R_2 on the flat surface. By combining these, the resultant R is obtained, which is decomposed into two main components: the tangential force X and the vertical reaction Z_R. This allows the formulation of equilibrium equations for the wheel, capturing the complex interactions between the wheel and the deformable track while maintaining a constant speed during the rolling process.

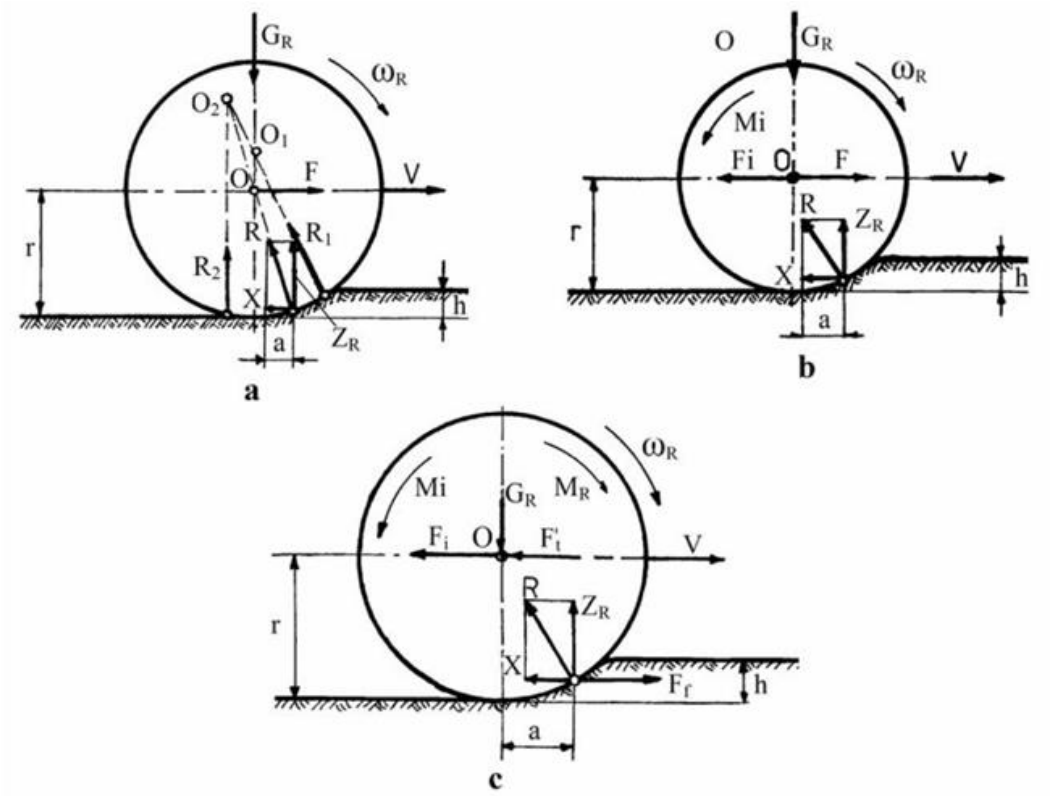

Fig. 8 - Wheel balance when traveling on a deformable roadway (Băisan, 2020)

In this case the tangential reaction is:

$$X = F = Z_r \frac{a}{r} = G_r f = R_r \text{ [N]} \tag{5}$$

If the inertial force is also considered:

$$\mathrm{X} = F - F_i = F - m_R \frac{dV}{dt} \text{ [N]} \tag{6}$$

To obtain the power balance, the inertia force (F_i), the translational speed of the wheel (V), are entered into relation (6):

$$V = \omega_R r \text{ [m/s]} \tag{7}$$

$$FV = M_r \omega_R + M_i \omega_R + F_i V \tag{8}$$

For the case where the wheel runs on deformable terrain at variable speed, the equilibrium equations are:

$$F_t - X - F_t' - F_i = 0 \tag{9}$$

$$Z_R - G_R = 0 \quad (10)$$

$$M_R - F_i\, r - M_i = 0 \quad (11)$$

where: F_t – traction force [N]; M_R – torque at the wheel [Nm]; M_i – moment of inertia [Nm]; F'_t – traction force reaction [N].

In the case of movement with constant speed F_i = 0 and M_i = 0, and the torque required for movement (M_R) is:

$$M_R = F_t r + M_i \text{ [Nm]} \quad (12)$$

$$r = \frac{V}{\omega_r} \text{ [m]} \quad (13)$$

In relation (12) add slip and theoretical speed (V_t), substitute r from relation (13) and F_t, and get:

$$M_R\omega_R = F_t(V_t - V) + XV + F'_t + FiV + M_i\omega_R \text{ [Nm]} \quad (14)$$

The deceleration is introduced into the calculations and it is obtained:

$$M_R\omega_R = F_t(V_t - V) + XV + F'_t \pm FiV \pm M_i\omega_R \text{ [Nm]} \quad (15)$$

It can be seen that the motor power required at the driving wheel ($M_R\omega_R$), in the context of variable speed travel on a deformable raceway, consists of the sum of the powers lost by the slippage of the driving wheel for running (XV), to imprint an accelerated motion (F_iV), and for an accelerated rotational movement ($M_i\omega_R$), respectively the power transmitted to the vehicle body (F_tV).

Depending on the characteristics of the raceway, at the point of contact with the tire, it is possible to manifest a maximum adhesion force. The ratio of this force to the normal reaction at the wheel is defined by the adhesion coefficient (φ) (*Băisan, 2020):*

$$\varphi = \frac{X_{max}}{Z_R} \Leftrightarrow X_{max} = \varphi Z_R \quad (16)$$

For the maximum grip force, a maximum moment at the driving wheels ($M_{R\,max}$) results, corresponding to a maximum force at the grip limit ($F_{R\,max}$).

$$M_{R\,max} = r_d\,(\varphi + f)Z_R \text{ [Nm]} \quad (17)$$

$$F_{R\,max} = \frac{M_{R\,max}}{r_d} = (\varphi + f\,)\,Z_R \text{ [N]} \quad (18)$$

In the situation where the vehicle has more than one driven wheel, the evaluation of the maximum adhesion force involves the use of the adhesion weight (G_{ad}), representing the sum of the normal reactions of the roadway on the driven wheels:

$$X_{max} = \varphi G_{ad} \text{ [N]} \quad (19)$$

When the movement takes place on an inclined terrain the maximum motor torque and the maximum force at the motor wheels is:

$$M_{R\,max} = r_d(\varphi + f)G_{ad}\cos\alpha \text{ [Nm]} \quad (20)$$

$$F_{R\,max} = (\varphi + f\,)\,G_{ad}\cos\alpha \text{ [N]} \quad (21)$$

There is the situation when the moment at the wheel is minimal, namely when the adhesion force is zero:

$$M_{R\,min} = r_d f Z_R \text{ [Nm]} \quad (22)$$

The torque at the wheel must satisfy the following inequality:

$$M_{R\,min} < M_R \leq M_{R\,max} \tag{23}$$

Slippage of the drive wheel occurs when the drive torque is maximum, thus a relative frictional speed appears in the contact area of the tire with the ground. In the case of wheels subjected to brake action (the braking moment, M_f, may also occur), the relationship can be formulated as:

$$M_f = Xr_d - Z_R a \text{ [Nm]} \tag{24}$$

For maximum braking torque there is:

$$M_{f\,max} = \varphi r_d Z_R - Z_R a = Z_R r_d(\varphi - f) \text{ [Nm]} \tag{25}$$

The determination of rolling resistance involves the use of the coefficient of rolling resistance, denoted f and defined as the ratio of the adhesion coefficient (a) to the wheel radius (r_d). The rolling resistance coefficient exhibits an approximately linear increase with platform speed.

Due to the ability of a platform to move on various types of tracks, the coefficient of rolling resistance is influenced by a multitude of factors. For this reason, for mathematical purposes, average values were adopted, adjusted according to the specific condition of the running surface.

Traction force is dependent on the coefficient of friction (μ) between the tire and the running surface, along with the radial load exerted on the wheel (G_R). Its expression can be formulated as follows (*Băisan, 2020).*

$$F_t = \mu G_R + \sigma \Sigma_{i=1}^{n} A_{vi} \text{ [N]} \tag{26}$$

where: A_v – the projection area of each tire protrusion located on a vertical plane in the running surface; n – the number of protrusions of the tire that come into contact with the ground.

The traction force of the vehicle influences the adhesion weight utilization coefficient $\boldsymbol{\varphi}_{ad}$:

$$\varphi_{ad} = \frac{F_t}{G_{ad}} \tag{27}$$

For wheeled platforms the slip coefficient of the driving wheels is calculated with the relation (*Băisan, 2020):*

$$\delta = a\,\frac{F_t}{G_{ad}} + b\left(\frac{F_t}{G_{ad}}\right)^c \tag{28}$$

The coefficients a, b and c depend on the type of tire, the air pressure in the tire and the type of soil on which the platform moves, the usual values being presented in the specialized literature *(Băisan, 2020).*

In the context of the vehicle traveling on a deformable roadway, the evaluation of the adhesion coefficient requires consideration of the fact that the maximum traction force ($F_{t\,max}$), at which slippage of the driving wheels is considered acceptable ($\boldsymbol{\delta}_{ad}$), is defined as equal to X_{max}:

$$\varphi = \frac{X_{max}}{G_{ad}} = \frac{F_{t\,max}}{G_{ad}} \tag{29}$$

For a platform moving on a track inclined at an angle α at a speed V, the forces and moments acting on it can be observed in figure 9.

This figure shows the rolling resistance moments on each axle (M_{r1} and M_{r2}), the tangential reaction forces (X_1 and X_2), and the reaction forces from the track surface (Z_1 and Z_2) (*Băisan, 2020*).

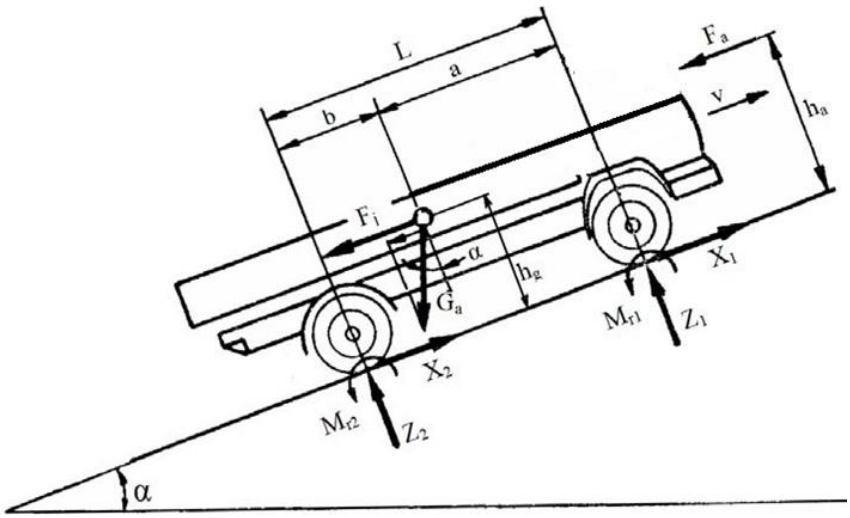

Fig. 9 - Diagram of forces and moments acting on the platform (Băisan, 2020)

The traction force at the wheel is determined using the following relationship (*Băisan, 2020*):

$$F_t = F_r + F_p + F_a + F_i = f G_a \cos\alpha + G_a \sin\alpha + C_x \frac{1}{2} A\rho v^2 + \frac{G_a}{g}\delta_{rot}\frac{dv}{dt} \text{ [N]} \quad (30)$$

The effective motor torque is calculated according to the following relationship:

$$M_e = \frac{P_m}{\omega} \text{ [Nm]} \quad (31)$$

In general cases, the balance of powers is determined with the help of the relationship (*Băisan, 2020*):

$$P_e = P_{tr} + P_r + P_p + P_i + P_a + P_\delta = F_t v\delta + \frac{vfG_a\cos\alpha}{10^3} + \frac{vG_a\sin\alpha}{10^3} + v\frac{G_a}{g}\frac{\delta_{rot}}{10^3}\frac{dv}{dt} + \frac{C_x A\rho v^3}{2*10^3} + \frac{\delta F_m v}{10^3(1-\delta)} \text{ [W]} \quad (32)$$

where: A – surface area exposed to air resistance [m^2]; F_t – traction force [N]; M_e – effective motor moment [Nm]; i_{tr} – total transmission ratio; η_{tr} – transmission efficiency[%]; r – wheel radius [m]; F_a – air resistance force [N]; F_p – the force required to climb the slope [N]; F_i – inertial force; F_r – rolling resistance force; C_x – aerodynamic coefficient; ρ – air density; G_a – total weight; v – speed [m/s]; α – the angle of inclination of the slope [degrees]; f– rolling resistance coefficient; δ– slip coefficient, δ_{rot} – coefficient of influence of the masses in the rotation movement; P_e – effective power [W]; P_{tr} – power lost during transmission; P_r – the power required to overcome the rolling resistance; P_p – the power required to climb the slope [W]; P_i – the power required to overcome the inertial force [W]; P_a – the power required to overcome the air resistance force [W]; P_δ – power lost during skating [W]; P_m – engine power [W]; ω – angular speed of the motor shaft [rad/s].

RESULTS

Calculating traction force in vehicle dynamics is essential for several key aspects of vehicle design, efficiency, and performance.

When calculating traction force for vehicles such as self-propelled platforms, some resistance forces are often neglected, for instance, air resistance, friction force in bearings or rollers, and in certain situations, even inertia force. These forces are not considered due to the reduced travel speed in such cases and the high gear ratios used, which greatly amplify the braking force when the engine is no longer accelerating (engine brake).

A crucial factor in calculating moments or forces at the wheel axis is the transmission. The transmission gear ratios must be known for each speed stage, as well as the final drive transmission, which can be a simple differential.

Currently, it is recommended that the engine force applied to the platform's propulsion system has a power reserve of at least 20%.

Case Study

In this simulation, the above relationships were used to calculate the minimum force needed for the movement of a self-propelled platform on a rigid surface with non-deformable wheels, intended for transporting loads up to a maximum of 2000 kg (load weight – 19613.3 N). The platform dimensions are (length x width x height, mm) – 4396 x 1848 x 1501, the mass of the platform – 1150 kg (weight – 11277,64 N), wheel radius - 0.295 m, total transmission ratio – 14.02, angle α ranging from 0 to 11.5 degrees, air density ρ = 1.225 kg/m³, transmission efficiency η_{tr} = 0.93, mass influence coefficient in rotational motion δ_{rot} = 1.144, considering dv/dt = 0.2 m/s², maximum travel speed – 2.2 m/s, aerodynamic coefficient C_x = 0.65, rolling resistance coefficient f = 0.0132, normal gravitational acceleration g = 9.806 m/s², A= 2.48 m² and sliding coefficient δ = 0.8-0.9 are known.

At the time of the experiment, the self-propelled platform is in the design stage, a car was used to validate the mathematical model. During the experiments, the maximum angle of the slope was 11.5 degrees and the measurement of the traction force was measured with the help of a dynamometer placed between the car and the tractor with which it was towed. The force at which the car starts moving was measured. Model optimization will be performed when the platform is ready for experimentation.

To calculate the traction force, relationship (30) was used, where all known data was substituted. The forces needed for movement were studied under two different operating conditions: when the platform is unloaded, and the propulsion system is used for movement on a horizontal surface, as well as on a surface with an incline ranging from 5 to 25 degrees. In the second case, the platform was loaded with the maximum proposed load under simulation conditions.

Table 1 presents the force values resulting from calculations when the platform is unloaded, and Table 2 shows the force values when the platform is loaded with the maximum load. The inertia force and the air resistance force have exceedingly small values and are typically neglected.

Table 1

Forces required for the movement of the self-propelled platform calculated for unloaded travel

F_t (N)	F_r (N)	F_p (N)	F_a (N)	F_i (N)	Angle α	Measured data F_t (N)
414.07	148.92	0.00	1.93	263.23	0.00	412.02
906.02	148.77	492.09	1.93	263.23	2.50	1098.72
1396.75	148.35	983.25	1.93	263.23	5.00	1294.92
1885.33	147.64	1472.53	1.93	263.23	7.50	1383.21
2660.25	145.93	2249.17	1.93	263.23	11.50	2266.11

Table 2

Forces required for the movement of the self-propelled platform calculated for travel with the maximum load

F'_t (N)	F'_r (N)	F'_p (N)	F'_a (N)	F'_i (N)	Angle α	Measured data F'_t (N)
561.64	202.40	0.00	1.48	357.76	0.00	558.86
1230.26	202.20	668.82	1.48	357.76	2.50	1491.93
1897.23	201.63	1336.36	1.48	357.76	5.00	1758.91
2561.27	200.66	2001.36	1.48	357.76	7.50	1879.13
3614.49	198.33	3056.91	1.48	357.76	11.50	3078.97

where:

F'_t - traction force (with maximum load) [N]; F'_r - rolling resistance force (with maximum load) [N]; F'_p - force required for uphill movement (with maximum load) [N]; F'_a - air resistance force [N]; F'_i - inertia force [N].

Figure 10 shows the graph with the variation of the forces required to move on horizontal ground or on a slope.

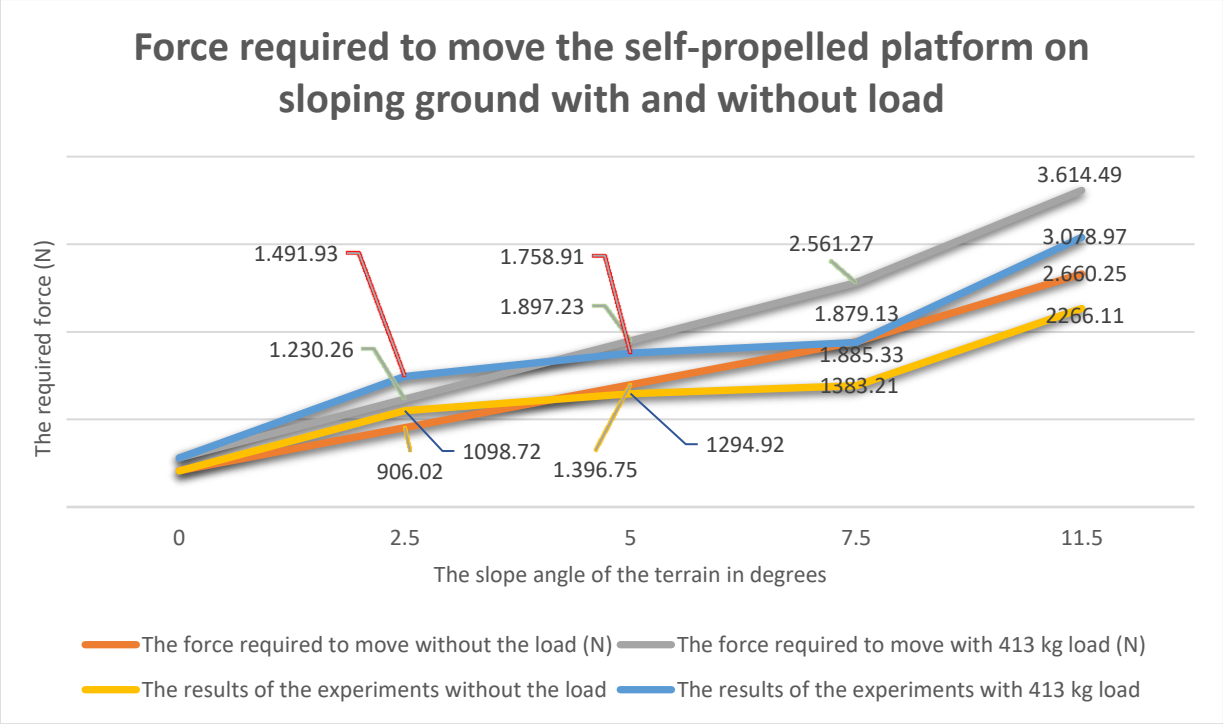

Fig. 10 – The graph with the variation of the forces as a function of the load and the slope angle

To calculate the power needed for displacement, relation (32) was used, all known data were replaced.

In tables 3 and 4, the values resulting from the calculations were entered, the same displacement conditions were used as in the case of determining the forces.

Table 3

Power required to move the self-propelled platform calculated for moving without load

P_e (W)	P_r (W)	P_p (W)	P_{tr} (W)	P_i (W)	P_a (W)	P_δ (W)	Angle α	Measured power P_e (W)
820.80	0.33	0.00	819.86	0.58	0.02	0.02	0.00	815.80
1795.99	0.33	1.08	1793.92	0.58	0.02	0.06	2.50	2175.47
2768.76	0.33	2.16	2765.57	0.58	0.02	0.10	5.00	2563.94
3737.26	0.33	3.24	3732.95	0.58	0.02	0.14	7.50	2738.76
5273.35	0.32	4.95	5267.29	0.58	0.02	0.18	11.50	4486.90

Table 4

Power required to move the self-propelled platform calculated for moving with full load

P'_e (W)	P'_r (W)	P'_p (W)	P'_{tr} (W)	P'_i (W)	P_a (W)	P'_δ (W)	Angle α	Measured power P'_e (W)
1112.52	0.13	0.00	1112.04	0.23	0.01	0.11	0.00	1106.54
2436.95	0.13	0.42	2435.92	0.23	0.01	0.24	2.50	2954.01
3758.10	0.13	0.85	3756.52	0.23	0.01	0.38	5.00	3482.64
5073.45	0.13	1.27	5071.31	0.23	0.01	0.51	7.50	3720.68
7159.71	0.13	1.94	7156.69	0.23	0.01	0.72	11.50	6096.36

where:

P'_e - effective power (with maximum load) [W]; P'_r - power required to overcome rolling resistance (with maximum load) [W]; P'_p - power required for uphill movement (with maximum load) [W]; P'_{tr} - power lost in transmission (with maximum load) [W]; P'_i - power required to overcome inertia force (with maximum load) [W]; P'_δ - power lost in slipping (with maximum load) [W].

Figure 11 shows the variation graph of the power required to move the self-propelled platform when moving on a horizontal or sloping ground with zero load or maximum load.

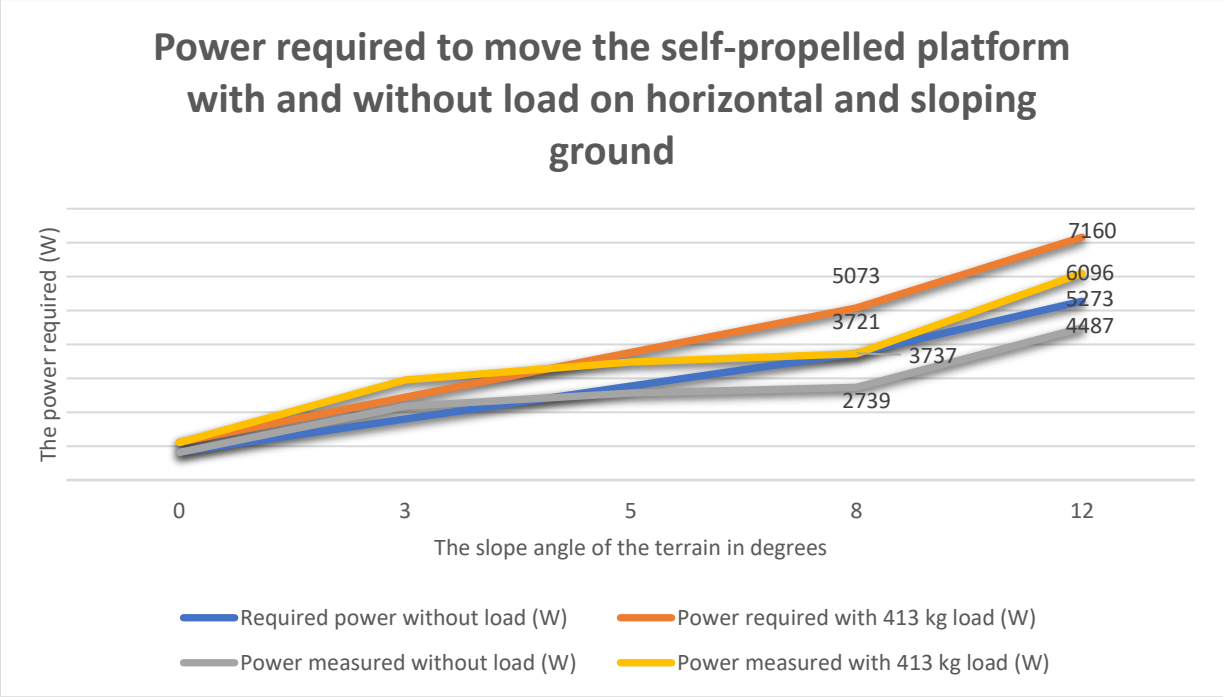

Fig. 11 – The graph with the variation of the power required to move the self-propelled platform in conditions of movement on a horizontal ground but also on a slope, without load but also with the maximum load

CONCLUSIONS

Self-propelled platforms represent a significant advancement in soil research, bringing forth numerous benefits. Technological advancements have transformed them into essential tools for the research community, facilitating the collection of precise data, optimizing research processes, and contributing to a deeper understanding of biogeochemical processes in the soil. The ongoing use of these platforms and the improvement of associated technologies will continue to support progress in soil research and the development of sustainable agricultural practices.

When calculating the power or force required for a motor to propel a platform, it is imperative to possess specific information about the vehicle's component subassemblies or those imposed by the project. The calculation method presented in this work is applicable to wheeled platforms with a 4x2 transmission, with travel speeds up to a maximum of 15 km/h, and a maximum mass not exceeding 2500 kg. In the case of these platform types, some of the resistance forces to movement are characterized by low values and can be neglected. Factors influencing the power of the propulsion system include the transmission, tire type, dimensions, and the platform's intended use. Following the necessary calculations, the power requirement interval for the motor, corresponding to the project's requirements, can be selected from the power requirement graphs.

The mathematical model presented in this paper proves to be a valuable tool in the design process of self-propelled platforms equipped with wheels. Its integration into the calculation algorithms of design software results in a significant reduction of the time required for simulation and the implementation of experimental models for these self-propelled platforms.

ACKNOWLEDGEMENT

This work was supported by the Romanian Research and Innovation Ministry, through the Project entitled: “An intelligent automated system designed for georeferenced soil sampling.” -- PN 23 04 01 02. Contract no./date 9N/ 01.01.2023.

REFERENCES

[1] Băisan I. (2020). Tractors, automobiles, and propulsion systems for agricultural machinery – Part I (Tractoare, automobile și sisteme de propulsie a mașinilor agricole – partea I), *documentary material for third-year students, specialization MIAIA*, "Gheorghe Asachi" Technical University, Faculty of Mechanics, Iași.

[2] Bulgakov V., Pascuzzi S., Santoro F., Anifantis A.S., (2018). Mathematical Model of the Plane-Parallel Movement of the Self-Propelled Root-Harvesting Machine. *Sustainability,* 2018, 10:3614.
[3] Cao X., Wang Z., Zheng B., Tan Y. (2023). Improved UAV-to-Ground Multi-Target Tracking Algorithm Based on StrongSORT, *Sensors (Basel, Switzerland)*, vol. 23, no. 22: 9239.
[4] Huuskonen J., Oksanen T. (2018). Soil sampling with drones and augmented reality in precision agriculture, *Computers and Electronics in Agriculture,* vol. 154, pp 25–35.
[5] Ibrahim A., Torres-Calderon W., Golparvar-Fard M. (2023). Reinforcement learning for high-quality reality mapping of indoor construction using unmanned ground vehicles, *Automation in Construction*, vol. 156.
[6] Li W., Yang F., Mao E., Shao M., Sui H., Du Y. (2022). Design and Verification of Crab Steering System for High Clearance Self-Propelled Sprayer. *Agriculture* 2022, 12, 1893.
[7] Oprescu R.M., Nenciu F., Voicea I., Cujbescu D., Persu C. (2023). Considerations for machinery used for mechanical weed control in organic farming*, ISB INMA TEH International Symposium*, pp. 600-611.
[8] Tan K.H., (2005) -Soil sampling, preparation and analysis, 2nd edition, *New York: CRC Press,* pp. 672, eBook ISBN 9780429178993.
[9] Vaeljaots E., Lehiste H., Kiik M., Leemet T. (2018). Soil sampling automation case-study using unmanned ground vehicle, *17th International Scientific Conference Engineering for Rural Development,* Jelgava, pp. 982-987.
[10] Vanghele N.A., Petre A. A., Matache A., Stanciu M.M, (2021) - Agriculture 5.0 - Review, *Annals of the University of Craiova,* vol. 51/2/2021, pp. 576-583.
[11] Vlăduţ V., Petre A., Voicea I., Matei Gh., Boruz S., Popa D, Isticioaia S., Biriș S. St, Ungureanu N., Epure M., Dumitru C., Atanasov At. (2020), Agriculture 4.0 - The Use of Smart Technologies for High-Performance Agriculture, *Annals of the University of Craiova - Agriculture, Montanology,* pp. 594-692.
[12] Zawilski B. M., Granouillac F., Claverie N., Lemaire B., Brut A., Tallec T., (2023). Calculation of soil water content using dielectric-permittivity-based sensors -- benefits of soil-specific calibration, *Geoscientific Instrumentation, Methods and Data Systems,* Vol. 12, pp. 45-56.
[13] *** https://www.mhnetwork.com/self-propelled-platform-truck-tug/
[14] *** https://argiles.es/informacion-producto/af5/?lang=en
[15] *** https://www.powermotiontech.com/sensors-software/automation/media-gallery/21254335/robotics-plus-unveils-unmanned-ground-vehicle-for-agricultural-operations?id=21254335&slide=2
[16] *** https://www.agriculture.com/news/technology/raven-announces-new-product-brand-and-autonomous-growth-platform
[17] *** https://hse-uav.com/products/r150-2023-autonomous-tractor-mower
[18] *** https://clearpathrobotics.com/blog/2021/01/husky-ugv-drives-smart-precision-agriculture-for-steep-slope-vineyards